Quantitative neuroimaging biomarkers in a series of 20 adult patients with POLG mutations

Marion Masingue, Isaac Mawusi Adanyeguh, Maya Tchikviladze, Thierry Maisonobe, Claude Jardel, Damien Galanaud, Fanny Mochel

Quantitative neuroimaging biomarkers in a series of 20 adult patients with *POLG* mutations

Marion Masingue[a,b], Isaac Adanyeguh[a], Maya Tchikviladzé[b], Thierry Maisonobe[c], Claude Jardel[d], Damien Galanaud[a,e], Fanny Mochel[a,f,g,*]

[a] *Sorbonne Université, UPMC-Paris 6, UMR S 1127 and Inserm U 1127, and CNRS UMR 7225, and Institut du Cerveau et de la Moelle épinière, F-75013, Paris, France*
[b] *AP-HP, Pitié-Salpêtrière University Hospital, Department of Neurology, Paris, France*
[c] *APHP, Pitié-Salpêtrière University Hospital, Department of Neurophysiology, Paris, France*
[d] *AP-HP, Pitié-Salpêtrière University Hospital, Metabolic Biochemistry Department, INSERM, U1016, Institut Cochin, Paris F-75014, France*
[e] *AP-HP, Pitié-Salpêtrière University Hospital, Department of Neuroradiology, Paris, France*
[f] *AP-HP, Pitié-Salpêtrière University Hospital, Department of Genetics, Paris, France*
[g] *University Pierre and Marie Curie, Neurometabolic Research Group, Paris, France*

A B S T R A C T

Mutations in the gene encoding polymerase gamma (POLG) are a common cause of mitochondrial diseases in adults. We retrospectively analyzed volumetric and diffusion tensor imaging data from 20 adult *POLG*-mutated patients compared to healthy controls. We used an original clinical binary load score and electroneuromyography to evaluate disease severity. Patients showed atrophy in the basal ganglia, amygdala, and brainstem ($p < 0.05$) compared to controls, as well as decreased fractional anisotropy (FA) in the cingulate gyrus, the internal capsule and the corona radiata ($p < 0.05$). Clinical scores correlated with decreased FA and increased radial diffusivity in several brain regions ($p < 0.05$).

1. Introduction

Clinical variability is major in neurometabolic disorders making their diagnosis difficult and, often, radiological findings are non-specific. Treatments are nonetheless emerging so that non-invasive techniques are needed to evaluate their efficacy. Furthermore, numerous works have shown that mitochondrial dysfunction plays an important role in the pathophysiology of neurodegenerative disorders such as Parkinson's disease or Huntington's disease (Mochel and Haller, 2011; Bose and Beal, 2016). Hence, identifying non-invasive biomarkers in *POLG*-mutated patients and other mitochondrial disorders could prove useful in the understanding of these rare neurometabolic disorders as well as more common neurological conditions.

The *POLG* gene encodes the catalytic subunit of the mitochondrial DNA polymerase gamma, the most important enzyme involved in mitochondrial DNA (mtDNA) replication and homeostasis. Patients with recessive *POLG* mutations have numerous clinical presentations and constitute one of the largest groups of mitochondrial diseases in adults (Lax et al., 2012). Neurological symptoms may include sensory neuronopathy, cerebellar impairment, movement disorders, oculomotor disorders, muscle weakness, cognitive or psychiatric symptoms, neurosensory impairment (hearing loss, cataract) and/or stroke-like episodes (Mochel and Haller, 2011). The diagnosis is guided by elevated lactate in blood and/or CSF, mitochondrial abnormalities on muscle biopsy – ragged red fibers, i.e. myofibers with abnormal mitochondria deposits, respiratory chain deficiencies, mtDNA deletions – and is confirmed by molecular analysis of the *POLG* gene. To date, there is no efficient treatment for *POLG*-mutated patients, though several therapeutic developments are in progress urging the need for biomarkers reflecting cerebral metabolism.

Findings on visual inspection of brain magnetic resonance imaging (MRI) – e.g. white matter abnormalities, sub-cortical atrophy and/or atrophy of the cerebellum, the brainstem and the corpus callosum, edema and ischemia (Van Goethem et al., 2004; Winterthun et al.,

Abbreviations: POLG, polymerage gamma; MRI/MRS, magnetic resonance imaging/spectroscopy; DTI, diffusion tensor imaging; FA, fractional anisotropy; RD, radial diffusivity; mtDNA, mitochondrial DNA; CSF, cerebrospinal fluid; TR, repetition time; TE, echo time; FOV, field of view; EMG, electroneuromyographic; ROI, region of interest; TBSS, tract-based spatial statistics

* Corresponding author at: Sorbonne Université, UPMC-Paris 6, UMR S 1127 and Inserm U 1127, and CNRS UMR 7225, and Institut du Cerveau et de la Moelle épinière, F-75013, Paris, France.

E-mail addresses: m.tchikviladze@hopital-foch.com (M. Tchikviladzé), thierry.maisonobe@aphp.fr (T. Maisonobe), claude.jardel@aphp.fr (C. Jardel), damien.galanaud@aphp.fr (D. Galanaud), fanny.mochel@upmc.fr (F. Mochel).

Oculomotor disorder	***(a+b)/2***	**/1**
Ptosis[a]	/1	
Ophtalmoplegia[b]	/1	
Neuropathy		**/1**
Cerebellar Impairment	***(c+d+e)/3***	**/1**
Ataxia[c]	/1	
Dysmetria[d]	/1	
Dysarthria[e]	/1	
Movement disorders	***(f+g+h+i+j)/5***	**/1**
Dystonia[f]	/1	
Tremor[g]	/1	
Myoclonus[h]	/1	
Chorea[i]	/1	
Hypokinesia[j]	/1	
Muscle weakness	***(k+l+m)/3***	**/1**
UL weakness[k]	/1	
LL weakness[l]	/1	
Axial weakness[m]	/1	
Pyramidal tract signs		**/1**
Cognitive impairment		**/1**
Psychiatric disorder		**/1**
Epilepsy		**/1**
Hypoacousia		**/1**
Total score		**/10**

Fig. 1. Clinical load of POLG-mutated patients. *UL: upper limbs, LL: lower limbs.*

Table 1
Clinical and demographic characteristics of *POLG*-mutated patients.

	Volumetry (n = 20)	DTI (n = 14)
Age (y)	49 ± 16 (14–73)	54 ± 14 (24–73)
Age at onset	30 ± 16 (0–57)	32 ± 16 (6–57)
Disease evolution prior to MRI	20 ± 15 (1–51)	21 ± 15 (1–51)
Sex-ratio (M/F)	8/12	5/9
Clinical load score	4.9 ± 1.1 (2.7–6.7)	4.7 ± 1.2 (2.7–6.7)

Data are presented as mean ± standard deviation (range). y: year; M: male; F: female.

2005; Echaniz-Laguna et al., 2010; Kurt et al., 2010; Saneto et al., 2010; Habek et al., 2012; Synofzik et al., 2012; Cheldi et al., 2013; Kinghorn et al., 2013; Sidiropoulos et al., 2013; Uusimaa et al., 2013; Degos et al., 2014; Bindu et al., 2015; Lam et al., 2015; Tchikviladzé et al., 2015; Henao et al., 2016; Janssen et al., 2016; Martikainen et al., 2016) – are not specific to *POLG* mutations and MRI can also be normal. Only one research study has reported changes in magnetic resonance spectroscopy (MRS) and diffusion tensor imaging (DTI) in *POLG*-mutated patients, but it was restricted to stroke-like episodes (Tzoulis et al., 2010) that only a subset of patients present with. Yet, obtaining quantitative cerebral measures is key to understand the pathophysiology of the neurometabolic alterations associated with *POLG* mutations and monitor the course of the disease despite its clinical heterogeneity. MRI techniques seem particularly suited to identify biomarkers reflecting brain metabolism (Bonvento et al., 2017). Likewise, cerebral volumetry is a longstanding tool in biomarkers neuroimaging studies in order to quantify the rate at which the brain changes or atrophies due to the disease or in response to therapy. Moreover, DTI allows to further assess the integrity of nerve fibers and hence gives some explanation on the underlying microstructure changes that results in the gross volume changes. This retrospective study therefore aimed at identifying biomarkers using both volumetry and DTI on a series of 20 adult *POLG*-mutated patients.

2. Material and methods

2.1. Patients and controls

Initial and follow-up data were obtained retrospectively from patients followed in rare disease reference centers at La Pitié-Salpêtrière hospital between 2003 and 2015. All participants provided their written informed consent for study procedures and data reporting. The *POLG* gene was sequenced as described (Whybra et al., 2004). The retrospective nature of our study prevented us from using clinical scales used in mitochondrial diseases, such as NMDAS (Newcastle Mitochondrial Disease Adult Scale). Yet, disease severity was assessed by an original clinical binary load score (Fig. 1). Likewise, we used previous clinical descriptions of *POLG*-mutated patients (Tchikviladzé et al., 2015) and listed the main symptoms susceptible to be present in our patient series. Symptoms belonging to the same neurological category were grouped in order to ensure that each neurological dysfunction weighed equally in the score. For example, dysarthria, dysmetria, and ataxia, all attributable to cerebellar impairment, were summed and divided by 3 so that the cerebellar score ranged from 0 to 1. This scale has never been used before in mitochondrial diseases. However, such binary scoring systems have been validated before in rare neurometabolic diseases (Whybra et al., 2004). Here, the overall score ranged from 0 (best) to 10 (worst). Two items – cerebellar impairment and movement disorders – were used as subscores and continuous variables for correlation purposes. Controls were healthy subjects who belonged to a control cohort selected for a previous DTI study (Van der Eerden

Table 2
Detailed mutations and clinical symptoms of the 20 *POLG*-mutated patients.

Patient	Sex	Age at onset	Age at first MRI	Mutation	Clinical symptoms Main (bold)/additional (italics)
1	F	48	73	c.1760C > T (p.Pro587Leu)[a] c.911 T > G (p.Leu304Arg)	SANDO Hearing loss
2	F	14	55	c.1760C > T (p.Pro587Leu)[a] c.1760C > T (p.Pro587Leu)[a]	SANDO Movement disorder, Depression
3	F	44	49	c.264C > G (p.Phe88leu) c.2243G > C (p.Trp748Ser)	MEMSA Cerebellar ataxia, Cognitive decline
4	F	6	26	c.235C > T (p.Leu79Phe) c.895A > C (p.Met299Leu)	MEMSA Pseudo-stroke
5	M	49	55	c.1943C > G (p.Pro648Arg) c.3286C > T (p.Arg1096Cys)	SANDO
6	F	16	48	c.428C > T (p.Ala143Val) c.2243G > C (p.Trp748Ser)	SANDO Pyramidal syndrome, Depression
7	M	40	63	c.1760C > T (p.Pro587Leu)[a] c.2542G > A (p.Gly848Ser)	SANDO
8	F	23	37	c.2554C > T (p.Arg852Cys) c.2665G > A (p.Ala889Thr)	MEMSA Cerebellar Ataxia
9	M	15	51	c.1399G > A (p.Ala467Thr) c.1399G > A (p.Ala467Thr)	SANDO
10	M	39	69	c.1760C > T (p.Pro587Leu)[a] c.2566G > A (p.Glu856Lys)	CPEO plus Peripheral neuropathy
11	F	21	72	c.1760C > T (p.Pro587Leu)[a] c.2566G > A (p.Glu856Lys)	CPEO plus Peripheral neuropathy
12	M	57	61	c.803G > C (p.Gly268Ala)[b]	SANDO Glomerulopathy
13	F	0	24	c.264C > G (p.Phe88Leu) c.856-6_856-4del	MIRAS Peripheral neuropathy, Hearing loss
14	M	33	45	c.2828G > A (p.Arg943His)[b]	SANDO Parkinsonism, Hearing loss Cataract, Optic atrophy
15	F	16	50	c.2864A > G (p.Tyr955Cys)[b]	SANDO Depression
16	F	24	33	c.2243G > C (p.Trp748Ser) c.2243G > C (p.Trp748Ser)	MEMSA
17	F	41	43	c.2243G > C (p.Trp748Ser) c.2243G > C (p.Trp748Ser)	SANDO Palatal tremor
18	F	46	47	c.2756 T > C (p.Met919Thr) c.2956 T > G (p.Tyr986Asp)	SANDO Hearing loss, Cataract
19	M	31	40	c.2243G > C (p.Trp748Ser) c.2243G > C (p.Trp748Ser)	SANDO Hearing loss, Cognitive decline Pyramidal syndrome, Depression
20	M	NA	NA	c.2243G > C (p.Trp748Ser) c.3286C > T (p.Arg1096Cys)	MIRAS

SANDO: sensory ataxia neuropathy dysarthria and ophthalmoplegia; MEMSA: myoclonic epilepsy myopathy sensory ataxia; CPEO: chronic progressive external ophthalmoplegia; MIRAS: mitochondrial recessive ataxia syndrome; NA: non available.

[a] In cis with polymorphism c.752C > T (p.Thr251Ile).

[b] The pathogenicity of these mutations have been discussed in Tchikviladzé et al., 2015 (Table e-1).

Table 3
Brain atrophy in *POLG*-mutated patients compared to controls.

ROI	*POLG*-mutated patients	Controls	*p* value
Global mean	0.0057 ± 0.0011 [0.0040–0.0084]	0.0073 ± 0.0009 [0.0048–0.0088]	< 0.001
Pallidum	0.016 ± 0.0004 [0.0012–0.0026]	0.0021 ± 0.0003 [0.0015–0.0025]	< 0.001
Caudate nucleus	0.0040 ± 0.00007 [0.0027–0.0054]	0.0049 ± 0.0004 [0.0042–0.0056]	< 0.001
Thalamus	0.0086 ± 0.012 [0.0064–0.0113]	0.0099 ± 0.0006 [0.0087–0.0111]	< 0.001
Accumbens nucleus	0.0006 ± 0.0001 [0.0004–0.0009]	0.0008 ± 0.00001 [0.0006–0.0011]	< 0.001
Amygdala	0.0018 ± 0.0003 [0.0014–0.0024]	0.0020 ± 0.0003 [0.0017–0.0025]	0.003
Brainstem	0.0125 ± 0.0013 [0.0093–0.0153]	0.0146 ± 0.0012 [0.0131–0.0170]	< 0.001

ROI analysis found significantly decreased adjusted volumes in *POLG*-mutated patients in basal ganglia, amygdala and brainstem. Data are presented as mean ± standard deviation [range].

et al., 2014).

2.2. Brain imaging

MRI acquisitions were performed on 1.5 and 3 T MR units (General Electric, WI, USA) using the standardized protocol used in our institution for the exploration of neuro metabolic diseases. Some *POLG*-mutated patients had a follow-up exam after 4 years. A 3D T1-weighted sequence (TR = 9.5 ms, TE = 3 ms, field of view (FOV) = 256 × 256 (n = 5), 512 × 512 (n = 15), matrix = 170 × 170 (n = 2), 180 × 180 (n = 3), 360 × 360 (n = 15)) was acquired for localization of brain regions and volumetric analyses. To evaluate the integrity of white matter microstructure, DTI was performed in a subgroup of patients (n = 14) with *b* value = 1000 s/mm^2, 12 directions (6 directions in 2 patients), TR = 12,000 ms, TE = 80 ms, FOV = 256 × 256, slice thickness = 3 mm.

2.3. Quality control

MRI acquisitions were made as part of routine clinical follow-up. This induced, at times, loss of quality, precision and homogeneity

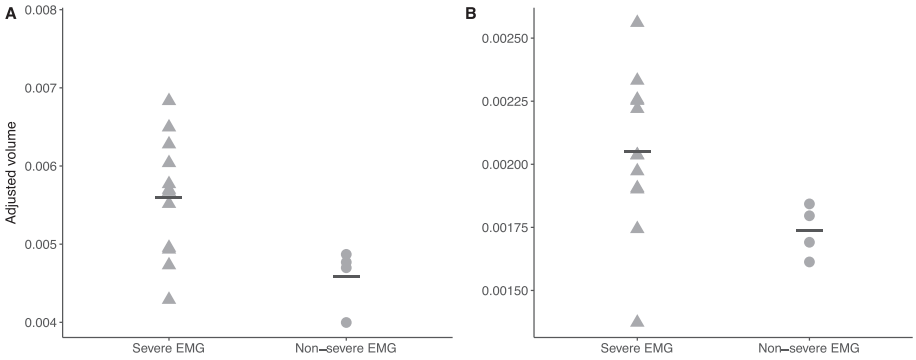

Fig. 2. Corpus callosum (A) and putamen (B) volumes in severely and non-severely affected patients on EMG. Severe EMG was defined as missing sensory potentials on lower and upper limbs. Patients with severe neuropathy had smaller corpus callosum ($p = .030$) and putamen ($p = .030$).

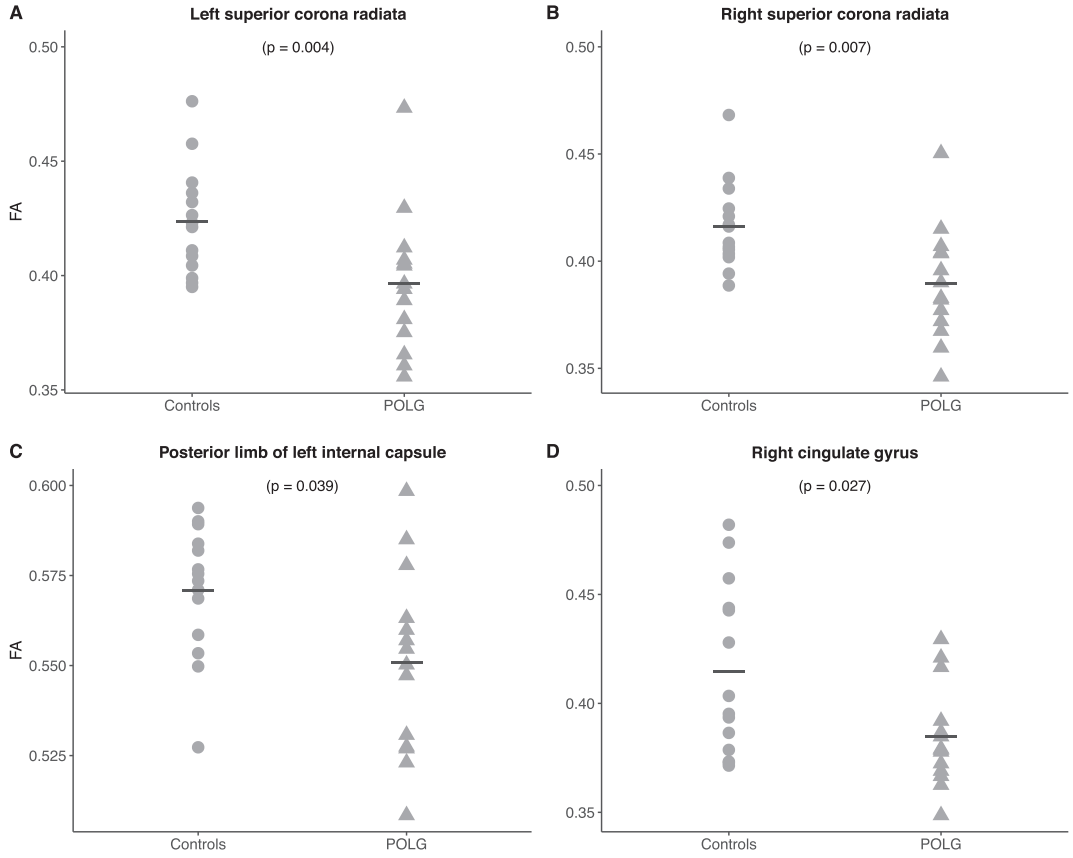

Fig. 3. FA values in *POLG*-mutated patients and controls. *POLG*-mutated patients had decreased FA compared to controls on the (A) left superior corona radiata ($p = .004$), (B) right superior corona radiata ($p = .007$), (C) left posterior limb of internal capsule ($p = .039$) and the (D) Right cingulate gyrus ($p = .027$).

compared to research MRI, as shown by the difference in FOV and matrix sizes between some images. After visual and manual control, images were not included if quality was inappropriate, i.e. (i) only axial or non-3D images making segmentation not possible or unreliable (n = 7), and/or (ii) images with severe motion artifacts (n = 1 for T1 and n = 0 for DTI).

2.4. Image analyses

We used the FMRIB Software Library (FSL) tools (http://www.fmrib.ox.ac.uk) for DTI analysis. The effects of head movement and eddy current-induced geometric distortions present on DTI images were corrected by eddy correction. After fitting the diffusion tensor model we generated maps of diffusion metrics – fractional anisotropy (FA) and radial diffusivity (RD). We performed tract based spatial statistics (TBSS) on FA and RD maps and used FSL's randomize for cross-subject voxel-wise statistics with multiple comparison correction. In addition, the JHU-atlas was used to extract the mean values of FA and RD for further analysis.

3D T1 volumetric images were automatically segmented for cortical and subcortical structures using FreeSurfer 5.3 (https://surfer.nmr.mgh.harvard.edu). We minimized the bias due to skull size differences by normalizing brain regions to the total intracranial volume of each subject to obtain the adjusted volume.

2.5. Electroneuromyography

Electroneuromyographic (EMG) studies were part of patients' follow-up. Sensory potential amplitudes and motor conduction velocities, motor distal latencies and composed action motor potentials

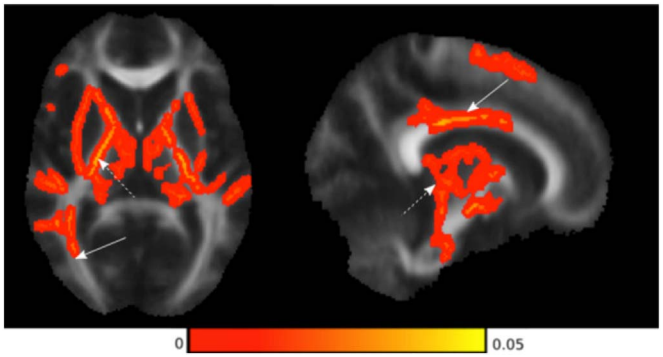

Fig. 4. Increased RD in *POLG*-mutated patients compared to controls. Statistical map using FSL-TBSS shows voxels with significantly increased RD in corona radiata (solid arrow – axial image), in the corpus callosum (solid arrow – sagittal image), the posterior thalamic radiations (dotted arrow – axial image) and the cerebral peduncles (dotted arrow – sagittal image).

amplitudes determined the type and the severity of neuropathy. Severe EMG profile was defined as the loss of sensory potentials on both lower and upper limbs, while maintained potentials in ulnar and/or radial nerves characterized non-severe EMG patterns.

2.6. Statistical analyses

Means were compared with the Mann and Whitney test and correlations were evaluated with Spearman coefficient. The Holm-Bonferroni step-down method of correction was applied for multiple tests.

3. Results

We gathered clinical and radiological data from 20 *POLG*-mutated patients. Their clinical and demographic characteristics are summarized in Table 1. The majority of our patients (n = 12) presented with SANDO (Table 2). Additionally, four patients presented with MEMSA, two patients with CPEO plus and two patients with MIRAS (Table 2). On visual inspection of brain MRI, only one patient displayed pseudo-strokes and no patient had Leigh syndrome. Two mutations were commonly found: c.2243G > C (p.Trp748Ser) in six patients, and c.1760C > T(Pro587Leu) – in cis with polymorphism c.752C > T (p.Thr251Ile) – in five patients, either at the homozygous or heterozygous state (Table 2). *POLG*-mutated patients were compared to 20 healthy controls. Four patients had a follow-up MRI after a 4-year interval. From the 16 *POLG*-mutated patients who had an EMG, 11 patients displayed a sensory neuronopathy while 5 presented with an axonal length-dependent neuropathy. The EMG was realized on average 1.4 (± 2.4) years before the MRI. Four patients had a severe EMG profile, defined as the loss of sensory potentials on both lower and upper limbs while non-severely affected patients had maintained potential in ulnar and/or radial nerve.

Brain volumetry showed a global atrophy in patients, especially in the hemispheric cortex, the basal ganglia, the amygdala, and the posterior part of the brainstem (Table 3). The 4 patients who had successive MRI showed a significant progression of atrophy in the right pallidum over time – adjusted volumes 0.00068 ± 0.00007 [0.00061–0.00075] versus 0.00101 ± 0.00018, [0.00079–0.00118] after 4 years, $p = 0.029$. The volume of the accumbens nuclei was different between patients with and without cognitive impairment – 0.00050 ± 0.00011 [0.00036–0.00072] versus 0.00061 ± 0.00007 [0.00051–0.00072], $p = 0.042$. There was also a trend towards a higher clinical score associated with smaller accumbens nuclei ($p = 0.130$), and higher cerebellar subscore along with smaller superior cerebellar peduncle ($p = 0.057$, data not shown). Patients with a severe neuropathy on EMG had significantly smaller corpus callosum and putamen than patients with a non-severe EMG profile (Fig. 2).

DTI analyses were available for 14 *POLG*-mutated patients. Their clinical and demographic characteristics are summarized in Table 1. Two patients had a follow-up DTI analysis after a 4-year interval. ROI analyses showed significantly decreased FA in the corona radiata, cingulate gyrus and internal capsule (Fig. 3). However, the mean global FA was not different between patients and controls – 0.4649 ± 0.0339, [0.4120–0.5354] versus 0.4677 ± 0.214, [0.4231–0.4990], $p = 0.607$. TBSS analyses displayed significantly increased RD in the corpus callosum, the superior longitudinal fasciculus, internal and external capsules and superior cerebellar peduncles (Fig. 4). The 2 patients with follow-up DTI exhibited a tendency to decreased FA in the corona radiata –2.223 ± 0.0336, [2.200–2.2470] versus 2.4196 ± 0.1194, [2.4112–2.4280], $p = 0.333$ – and in the anterior internal capsule – 0.8854 ± 0.3248, [0.8616–0.9065] versus. 0.9454 ± 0.0107, [0.9378–0.9529], $p = 0.333$. There was however no significant difference in RD in these two patients. The cerebellar subscore correlated with the FA in the cingulate gyrus (Spearman coefficient = −0.680, $p = 0.028$). Movement disorders were associated with increased RD in the internal capsule (Spearman coefficient = 0.745, $p = 0.006$) and the corona radiata (Spearman coefficient = 0.622, $p = 0.036$) while cerebellar impairment correlated with RD in the cerebral peduncle (Spearman coefficient = 0.613, $p = 0.040$) (Fig. 5). Patients with hypoacousia presented with a higher RD in the fornix than patients without hearing impairment – 0.0021 ± 0.0003 [0.0018–0.0026] versus 0.0017 ± 0.0002 [0.0014–0.0020], $p = 0.004$. There was no significant correlation between electrical parameters and DTI values.

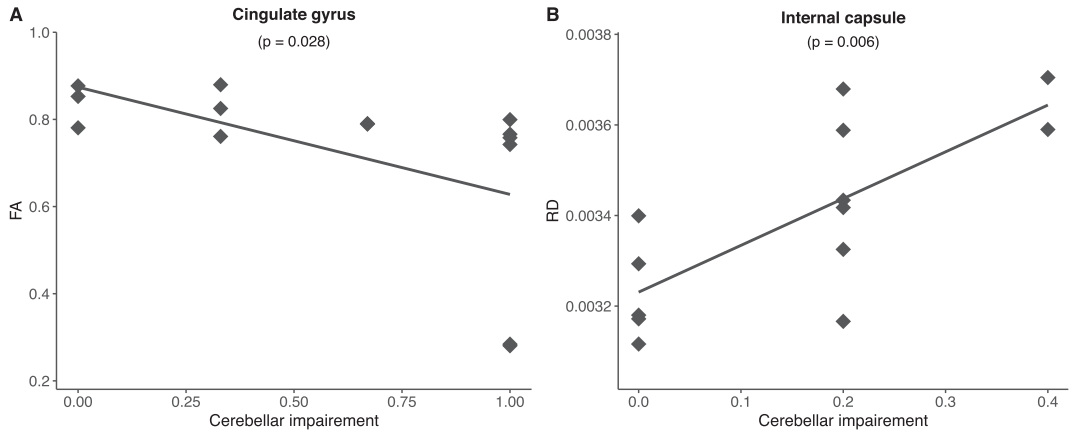

Fig. 5. Clinical correlation with DTI. (A) Cerebellar impairment correlated with low FA in the cingulate gyrus (Spearman coefficient = −0.680 $p = .028$) and (B) movement disorders with high RD in the internal capsule (Spearman coefficient = 0.745, $p = .006$).

4. Discussion

Our study shows that *POLG*-mutated patients displayed atrophy of the basal ganglia, amygdala and posterior cortex, consistent with the neurodegenerative process observed in adult patients. DTI also revealed abnormalities in the corona radiata, the internal capsule and the cingulate gyrus, possibly reflecting myelin alterations related to energy deficiency in *POLG*-mutated patients. Furthermore, to circumvent the wide and heterogeneous phenotypical spectrum that characterize *POLG*-mutated patients, we used an original binary clinical load, a method that has been validated before in rare neurometabolic diseases (Whybra et al., 2004). This score provided a simple homogenous clinical variable, which may prove useful in future studies but requires further validation. We also used EMG numerical data to evaluate disease severity since peripheral nerve involvement is very common in *POLG*-mutated patients.

This is the first study associating two structural and quantitative neuroimaging modalities on a large series of adult patients with *POLG* mutations. Up to now, brain atrophy in *POLG*-mutated patients has been reported on visual inspection only (Tchikviladzé et al., 2015) while our work provides quantified measures of brain atrophy. Notably, cerebellar impairment correlated with atrophy of the cingulate gyrus, and cognitive impairment appeared to be linked to smaller basal ganglia. Using DTI, we also found correlation between cerebellar impairment and FA in the corona radiata of *POLG*-mutated patients, as well as movement disorders and RD in the corona radiata and internal capsule. This clinical study also showed altered brain diffusion in key white matter regions (cingulate gyrus, corona radiata, internal capsule) that may reflect cerebral metabolic alterations. Those results were found using both TBSS and ROI analyses, emphasizing that DTI can be a reliable tool even when performed as part of clinical routine follow-up. This is consistent with our work in other neurometabolic disorders such as Niemann Pick type C disease where we showed that DTI can identify biomarkers of disease progression and response to treatment (Masingue et al., 2017).

This study has some methodological limitations. MRI acquisitions were performed in a clinical (and not research) setting leading to suboptimal data quality. However, the coherence between the DTI findings obtained from ROI and TBSS approaches suggests that DTI may be less susceptible to artifacts generated by clinical MRI. Another limitation of this study is the limited size of our patient population. Nevertheless, our work reports on more patients than previous MRI studies in *POLG*-mutated patients. It is also the first DTI study performed in the macroscopically normal–appearing cerebral parenchyma, unlike previous work conducted within white matter and/or pseudo-stroke lesions from *POLG*-mutated patients (Tzoulis et al., 2010).

5. Conclusion

Despite its methodological limits, this original work supports the use of MRI for the identification of biomarkers in *POLG*-mutated patients. Prospective studies are, however, needed to assess with disease progression the evolution of the volumetric and DTI parameters that we have identified.

Consent for publication

Not applicable (manuscript contains no individual person's data).

Competing interests

Authors declare no financial or non-financial competing interests in relation with this manuscript.

Funding sources for the study

MM was supported by the JNLF (Journées de Neurologie de langue Française) JNLF-SFN-ARSEP, 2015-2016.

Author contributions

MM and FM were involved in conception and design of the research project, analysis and interpretation of the data, and writing of the first draft of the manuscript. DG was involved in conception and design of the research project. MT was involved in the acquisition of clinical data, TM in the acquisition, analysis and interpretation of the EMG data and MM, IA, DG and FM in the acquisition, analysis and interpretation of the neuroimaging data. All authors read and approved the final manuscript.

Acknowledgments

We thank the following physicians for patients' referral: Sophie Demeret, Alexandra Durr, Karine Viala, Guillaume Bassez, Anthony Behin, Bruno Eymard, Pascal Laforêt, Yann Nadjar, Emmanuel Roze.

References

Bindu, P.S., Arvinda, H., Taly, A.B., Govindaraju, C., et al., 2015. Magnetic resonance imaging correlates of genetically characterized patients with mitochondrial disorders: a study from south India. Mitochondrion 25, 6–16.

Bonvento, G., Valette, J., Flament, J., Mochel, F., Brouillet, E., 2017. Imaging and spectroscopic approaches to probe brain energy metabolism dysfunction in neurodegenerative diseases. J. Cereb. Blood Flow Metab. 1, 271678X17697989. https://doi.org/10.1177/0271678X17697989.

Bose, A., Beal, M.F., 2016. Mitochondrial dysfunction in Parkinson's disease. J. Neurochem. 1, 216–231.

Cheldi, A., Ronchi, D., Bordoni, A., Bordo, B., et al., 2013. POLG1 mutations and stroke like episodes: a distinct clinical entity rather than an atypical MELAS syndrome. BMC Neurol. 13 (8). https://doi.org/10.1186/1471-2377-13-8.

Degos, B., Laforêt, P., Jardel, C., Sedel, F., et al., 2014. POLG mutations associated with remitting/relapsing neurological events. J. Clin. Neurosci. 21, 186–188.

Echaniz-Laguna, A., Chassagne, M., de Sèze, J., Mohr, M., Clerc-Renaud, P., Tranchant, C., Mousson de Camaret, B., 2010. POLG1 variations presenting as multiple sclerosis. Arch. Neurol. 67, 1140–1143.

Habek, M., Barun, B., Adamec, I., Mitrović, Z., Ozretić, D., Brinar, V.V., 2012. Early-onset ataxia with progressive external ophthalmoplegia associated with POLG mutation: autosomal recessive mitochondrial ataxic syndrome or SANDO? Neurologist 18, 287–289.

Henao, A.I., Pira, S., Herrera, D.A., Vargas, S.A., Montoya, J., Castillo, M., 2016. Characteristic brain MRI findings in ataxia-neuropathy spectrum related to POLG mutation. Neuroradiol. J. 29, 46–48.

Janssen, W., Quaegebeur, A., Van Goethem, G., Ann, L., Smets, K., Vandenberghe, R., Van Paesschen, W., 2016. The spectrum of epilepsy caused by POLG mutations. Acta Neurol. Belg. 116, 17–25.

Kinghorn, K.J., Kaliakatsos, M., Blakely, E.L., Taylor, R.W., Rich, P., Clarke, A., Omer, S., 2013. Hypertrophic olivary degeneration on magnetic resonance imaging in mitochondrial syndromes associated with POLG and SURF1 mutations. J. Neurol. 260, 3–9.

Kurt, B., Jaeken, J., Van Hove, J., Lagae, L., et al., 2010. A novel POLG gene mutation in 4 children with Alpers-like hepatocerebral syndromes. Arch. Neurol. 67, 239–244.

Lam, C.W., Law, C.Y., Siu, W.K., Fung, C.W., et al., 2015. Novel POLG mutation in a patient with sensory ataxia, neuropathy, ophthalmoparesis and stroke. Clin. Chim. Acta 448, 211–214.

Lax, N., Whittaker, R., Hepplewhite, P., Reeve, A., et al., 2012. Sensory neuropathy in patients harbouring recessive polymerase gamma mutations. Brain 135, 62–71.

Martikainen, M.H., Ng, Y.S., Gorman, G.S., Alston, C.L., et al., 2016. Clinical, genetic, and radiological features of extrapyramidal movement disorders in mitochondrial disease. JAMA Neurol. 73, 668–674.

Masingue, M., Adanyeguh, I., Nadjar, Y., Sedel, F., Galanaud, D., Mochel, F., 2017. Evolution of structural neuroimaging biomarkers in a series of adult patients with Niemann-Pick type C under treatment. Orphanet J. Rare Dis. 12, 22–28. https://doi.org/10.1186/s13023-017-0579-3.

Mochel, F., Haller, R.G., 2011. Energy deficit in Huntington disease: why it matters. J. Clin. Invest. 121, 493–499.

Saneto, R.P., Lee, I.C., Koenig, M.K., Bao, X., Weng, S.W., Naviaux, R.K., Wong, L.J., 2010. POLG DNA testing as an emerging standard of care before instituting valproic acid therapy for pediatric seizure disorders. Seizure 19, 140–146.

Sidiropoulos, C., Moro, E., Lang, A.E., 2013. Extensive intracranial calcifications in a patient with a novel polymerase γ-1 mutation. Neurology 81, 197–198.

Synofzik, M., Srulijes, K., Godau, J., Berg, D., Schöls, L., 2012. Characterizing POLG ataxia: clinics, electrophysiology and imaging. Cerebellum 11, 1002–1011.

Tchikviladzé, M., Gileron, M., Maisonobe, T., Galanaud, D., et al., 2015. A diagnostic flow-chart for POLG-related diseases based on signs sensitivity and specificity. J. Neurol. Neurosurg. Psychiatry 86, 646–654.
Tzoulis, C., Neckelmann, G., Mørk, S.J., Engelson, B.E., et al., 2010. Localized cerebral energy failure in DNA polymerase gamma-associated encephalopathy syndromes. Brain 133, 1428–1437.
Uusimaa, J., Gowda, V., McShane, A., Smith, C., et al., 2013. Prospective study of POLG mutations presenting in children with intractable epilepsy: prevalence and clinical features. Epilepsia 54, 1002–1011.
Van der Eerden, A.W., Khalilzadeh, O., Perlbarg, V., Dinkel, J., et al., 2014. White matter changes in comatose survivors of anoxic ischemic encephalopathy and traumatic brain injury: comparative diffusion-tensor imaging study. Radiology 270, 506–516.
Van Goethem, G., Luoma, P., Rantamäki, M., Al Memar, A., et al., 2004. POLG mutations in neurodegenerative disorders with ataxia but no muscle involvement. Neurology 63, 1251–1257.
Whybra, C., Kampmann, C., Krummenauer, F., Ries, M., et al., 2004. The Mainz Severity Score Index: a new instrument for quantifying the Anderson-Fabry disease phenotype and the response of patients to enzyme replacement therapy. Clin. Genet. 65, 299–307.
Winterthun, S., Ferrari, G., He, L., Taylor, R.W., et al., 2005. Autosomal recessive mitochondrial ataxic syndrome due to mitochondrial polymerase gamma mutations. Neurology 64, 1204–1208.